Acta Mech 229, 2657–2673 (2018)
https://doi.org/10.1007/s00707-018-2122-6

ORIGINAL PAPER

Kourosh Hasanpour · Davoud Mirzaei

A fast meshfree technique for the coupled thermoelasticity problem

Received: 5 June 2017 / Revised: 15 December 2017 / Published online: 1 March 2018

Abstract This paper concerns a new and fast meshfree method for the linear coupled thermoelasticity problem. The resulting algorithm provides an attractive alternative to existing mesh-based and meshfree methods. Compared with mesh-based methods, the proposed technique inherits the advantages of meshfree methods allowing the use of scattered points instead of a predefined mesh. Compared with the existing meshfree methods, the proposed technique is truly meshless, requiring no background mesh for both trial and test spaces and, more importantly, numerical integrations are done over low-degree polynomials rather than complicated shape functions. In fact, this method mimics the known advantages of both meshless and finite element methods, where in the former triangulation is not required for approximation and in the latter the stiffness and mass matrices are set up by integration against simple polynomials. The numerical results of the present work concern the thermal and mechanical shocks in a finite domain considering classical coupled theory of thermoelasticity.

1 Introduction

Thermoelasticity is the generalization of the classical theory of elasticity and of the theory of thermal conductivity which involves the study of the stresses and strains developed in a solid body due to temperature variations, principally via heat conduction, and the energy dissipation associated with heat flow. The fundamental relations and differential equations of thermoelasticity have been well formulated. Historically, two general theories are mainly used to address the thermoelastic problem, usually denoted as the *uncoupled* and *coupled* cases. The uncoupled case essentially deals with the theory of thermal stresses. The theory is based on the assumption to disregard the influence of deformations of the medium on the temperature field, but account for the influence of the temperature field, when calculating the stresses of the medium. On the other hand, in coupled thermoelasticity, all interactions are taken into account. When the inertia effects are included, both for the mechanical and thermal part, then it is dealing with fully coupled dynamic thermoelasticity [1,8,18].

As pointed at before, the theory of thermoelasticity is well established in past decades. Some analytical and close-form solutions in special situations exist [8,11,12,18,21,22]. The fundamental matrix solution of the system of partial differential operators that governs the diffusion of heat and the strains in elastic media is

K. Hasanpour
Department of Mechanical Engineering, Faculty of Engineering, University of Isfahan, P.O. Box 81746-73441, Isfahan, Iran
E-mail: hasanpour@eng.ui.ac.ir

D. Mirzaei (✉)
Department of Mathematics, University of Isfahan, P.O. Box 81746-73441, Isfahan, Iran
E-mail: d.mirzaei@sci.ui.ac.ir

D. Mirzaei
Department of Mathematics, Khansar Faculty of Mathematics and Computer Science, Khansar 87916-85163, Iran

given in [31]. Numerical solutions through the finite elements method (FEM) have been reported by several authors [5,8,17,19,27]. The boundary elements method (BEM) has also been successfully applied to coupled and uncoupled thermoelastic problems [6,8,10,25,26,28,30].

More recently, some variations of meshless techniques are applied to solve problems concerning the propagation of thermoelastic waves. In [23] the meshless formulation based on local boundary integral equation (LBIE) methods was presented for some two-dimensional uncoupled thermoelastic problems. The meshless local Petrov–Galerkin method (MLPG) has been applied in transient linear thermoelastic analysis for orthotropic material properties in [24]. MLPG methods with different trial approximations have been used for variations of linear uncoupled and coupled thermoelastic problems in [7,20,33]. The shape optimization of linear thermoelastic solids is considered in [4] using a meshless approximation technique.

Although MLPG is known as a *truly* meshfree method, it still suffers from the cost of numerical integration. In MLPG (and many other meshfree methods) the stiffness and mass matrices are formed by integration against the moving least squares (MLS) shape functions and their derivatives which are complicated to evaluate, compared with the classical FEM where the integrands are low-degree and close-form polynomials. This disadvantage might be overcome by a simple and useful modification [15] which uses the concept of generalized moving least squares (GMLS) approximation [16] to shift the numerical integrations over low-degree polynomial basis functions. In another point of view, the new method bypasses the shape functions and *directly* approximates the PDE operators from nodal values. Thus it is called the Direct MLPG, or simply DMLPG. The new method generalizes the finite differences method (FDM) for scattered point layouts.

In this paper we apply the DMLPG method for solving the coupled thermoelastic problem.

The remainder of this paper is organized as follows. In Sect. 2 the MLS and the GMLS approximations are reviewed. The governing equations of thermoelasticity are given in Sect. 3. In Sect. 4 the local weak forms of thermoelastic equation are derived, and in Sect. 5 the GMLS approximation is applied to local weak forms. Finally, in Sect. 6 some numerical results are presented.

2 The meshfree approximation method

Let $\Omega \subset \mathbb{R}^d$, for positive integer d, be a nonempty and bounded set. Following the principle of meshfree methods which write solutions entirely in terms of scattered nodes, assume that

$$X = \{x_1, x_2, \ldots, x_N\} \subset \Omega$$

is a set containing N points in Ω. The quality of the point set X is measured by the *fill distance* defined by

$$h := h_{X,\Omega} = \sup_{x\in\Omega} \min_{1\leqslant j\leqslant N} \|x - x_j\|_2,$$

and the *separation distance* defined by

$$q_X = \frac{1}{2} \min_{i\neq j} \|x_i - x_j\|_2,$$

where $\|\cdot\|_2$ is the Euclidian norm. The fill distance is the radius of the largest open ball with center in Ω that contains none of the centers x_j from X. The separation distance is the largest possible radius for two balls centered at different points to be essentially disjoint. A set X of points is said to be *quasi-uniform* with respect to a constant $c_{\mathrm{qu}} > 0$ if

$$q_X \leqslant h_{X,\Omega} \leqslant c_{\mathrm{qu}} q_X. \tag{1}$$

Henceforth, we use the notation $\mathbb{P}_m^d$, $m \in \mathbb{N}_0 = \{n \in \mathbb{Z}, n \geqslant 0\}$, for the space of d-variable polynomials of degree at most m of dimension $Q := \binom{m+d}{d}$. A basis for this space is denoted by $\{p_1, \ldots, p_Q\}$.

A set $X = \{x_1, \ldots, x_N\} \subset \mathbb{R}^d$ with $N \geqslant Q$ is called $\mathbb{P}_m^d$-unisolvent if the zero polynomial is the only polynomial from $\mathbb{P}_m^d$ that vanishes on X.

Different meshfree approximation methods are available in the literature. We focus on the *moving least squares (MLS) approximation* and its variations in this paper. Let $u \in C^{m+1}(\Omega)$ be a function or a solution of a

patrial differential equation to be approximated. For a sample point $x \in \Omega$ the MLS provides an approximation $\widehat{u}(x)$ of $u(x)$ in terms of nodal values $u(x_j)$ by

$$u(x) \approx \widehat{u}(x) = \sum_{j=1}^{N} a_j(x) u(x_j), \quad x \in \Omega, \tag{2}$$

where $a_j(x)$ are *MLS shape functions* given by

$$a_j(x) = w(x, x_j) \sum_{k=1}^{Q} \alpha_k(x) p_k(x_j),$$

where the influence of the centers is governed by a weight function $w_j(x) = w(x, x_j)$, which vanishes for arguments $x, x_j \in \Omega$ with $\|x - x_j\|_2$ greater than a certain threshold, say δ. Thus we can define $w_j(x) = K((x - x_j)/\delta)$ where $K : \mathbb{R}^d \to \mathbb{R}$ is a nonnegative function with support in the unit ball $B(0, 1)$. The coefficients $\alpha_k(x)$ are the unique solution of

$$\sum_{k=1}^{Q} \alpha_k(x) \sum_{j \in I(x)} w_j(x) p_k(x_j) p_\ell(x_j) = p_\ell(x), \quad 0 \leqslant \ell \leqslant Q,$$

where $I(x) = \{j : \|x - x_j\|_2 \leqslant \delta\}$ is the family of indices of points in the support of the weight function. In vector form,

$$\boldsymbol{a}(x) = W(x) P^T(x) [P(x) W(x) P^T(x)]^{-1} \boldsymbol{p}(x), \tag{3}$$

where $W(x)$ is the diagonal matrix carrying the weights $w_j(x)$ on its diagonal, $P(x)$ is a $Q \times \#I(x)$ matrix of values $p_k(x_j)$, $j \in I(x)$, $1 \leqslant k \leqslant Q$, and $\boldsymbol{p} = (p_1, \ldots, p_Q)^T$. The matrix P depends on the evaluation point x via the index family $I(x)$. In MLS, one finds the best approximation to u at point x out of $\mathbb{P}_m^d$ with respect to a discrete ℓ^2 norm induced by a *moving* inner product, where the corresponding weight function depends not only on the points x_j but also on the evaluation point x in question [13]. If for every $x \in \Omega$ the set $\{x_j : j \in I(x)\}$ is $\mathbb{P}_m^d$-unisolvent then $A(x) = P(x) W(x) P^T(x)$ is a symmetric positive definite matrix. More details can be found in Chapter 4 of [32]. In what follows we will assume that K is nonnegative and continuous on $\mathbb{R}^d$ and supported on the ball $B(0, 1)$. In many applications, we can assume that

$$K(x) = \varphi(\|x\|_2), \quad x \in \mathbb{R}^d,$$

meaning that K is a radial function. Here $\varphi : [0, \infty) \to \mathbb{R}$ is positive and supported in $[0, 1]$ and its even extension is nonnegative and continuous on $\mathbb{R}$. If we assume that $K \in C^k(\mathbb{R}^d)$ then $a_j \in C^n(\Omega)$ where $n = \min\{k, m\}$. This implies that $\widehat{u} \in C^n(\Omega)$.

This approximation method can be used for solving partial differential equations (PDE). For this purpose, there exist two possibilities which we call the *trial function* and the *direct* approach. Assume

$$Lu = f$$

is an abstract PDE model which represents a PDE in a strong or a weak form. In the trial function approach, u is first approximated by $\widehat{u}$ and then the differential or integral operator L is applied to $\widehat{u}$. Thus, the values $La_j(x)$ have to be calculated. This is a very time-consuming task, especially when L contains higher order derivatives or when a numerical integration is required for weak-form cases. See the process of calculating a_j ending with Eq. (3) and guess how difficult the calculation of La_j would be. The trial function approach has been used extensively in meshfree methods; see for example [2,3].

The second approach (the direct approach), which was first introduced in [15,16] in the context of meshfree methods, bypasses the trial space and directly approximates Lu from nodal values $u(x_j)$:

$$Lu(x) \approx \widehat{Lu}(x) = \sum_{j=1}^{N} a_j^L(x) u(x_j), \quad x \in \Omega, \tag{4}$$

where $a_j^L(x)$ are given by

$$a_j^L(x) = w(x, x_j) \sum_{k=1}^{Q} \alpha_k^L(x) p_k(x_j).$$

Here the coefficients $\alpha_k^L(x)$ are the unique solution of

$$\sum_{k=1}^{Q} \alpha_k^L(x) \sum_{j \in I(x)} w_j(x) p_k(x_j) p_\ell(x_j) = Lp_\ell(x), \quad 0 \leqslant \ell \leqslant Q.$$

Thus in matrix form we have

$$\boldsymbol{a}^L(x) = W(x)P^T(x)[P(x)W(x)P^T(x)]^{-1} L\boldsymbol{p}(x). \tag{5}$$

Of course, $\boldsymbol{a}^L(x)$ is different from $L\boldsymbol{a}(x) = L\{W(x)P^T(x)[P(x)W(x)P^T(x)]^{-1}\boldsymbol{p}(x)\}$ for a nonidentity operator L. Since the new approach generalizes the classical MLS approximation (4) to approximate $Lu(x)$ from nodal values, it was called the *generalized moving least squares (GMLS) approximation* in [16]. As we can see from (5), L has to be evaluated only on polynomial basis functions p_ℓ instead of the complicated MLS shape functions a_j. This significantly reduces the computational cost of numerical meshfree algorithms based on MLS approximation. It is surprising that this modification does not affect the rate of convergence of the approximated function toward the exact solution. Theoretical results are given in [16].

In the following sections, we introduce a local weak-form scheme based on this new approximation technique to solve a coupled thermoelastic problem.

To stabilize the GMLS algorithm, instead of $\{(\cdot)^\alpha\}_{0\leq|\alpha|\leq m}$, the *shifted* and *scaled* polynomial basis functions

$$\left\{ \frac{(\cdot - x)^\alpha}{h_{X,\Omega}^{|\alpha|}} \right\}_{0\leq|\alpha|\leq m}$$

are used as a basis for $\mathbb{P}_m^d$ at a sample point $x \in \Omega$. This shifts the basis functions to each local subdomain to improve the accuracy, and scales the moment matrix $A(x)$ to get a constant condition number independent of $h_{X,\Omega}$. Here $\alpha = (\alpha_1, \ldots, \alpha_d) \in \mathbb{N}_0^d$ ($\mathbb{N}_0 = \mathbb{N} \cup \{0\}$) is a multi-index and $|\alpha| = \alpha_1 + \cdots + \alpha_d$.

3 Governing equations in thermoelasticity

In this section, we recall the governing equations of the dynamic coupled thermoelasticity problem for a homogeneous isotropic solid. Let Ω be a finite domain with boundary Γ. The basic equations of linear coupled thermoelasticity in absence of body forces and heat flux can be written as

$$\sigma_{ij,j} - \rho\ddot{u}_i = 0, \tag{6}$$

$$\kappa\theta_{,ii} - \rho c_e\dot{\theta} - \gamma\theta_0\dot{u}_{j,j} = 0, \tag{7}$$

where the constitutive equation is

$$\sigma_{ij} = 2\mu\varepsilon_{kl} + \lambda\varepsilon_{kk}\delta_{ij} - \gamma\theta\delta_{ij},$$

in which

$$\varepsilon_{ij} = \frac{1}{2}\big(u_{i,j} + u_{j,i}\big).$$

In the above equations σ_{ij}, u_i, ε_{ij}, γ, θ, θ_0, ρ, c_e and κ are the Cauchy tensor, component of displacement vector, strain tensor, stress-temperature modulus, absolute temperature, reference temperature, mass density, specific heat and conductivity, respectively, and λ and μ are Lamé constants. In addition δ_{ij} is the Kronecker delta function.

First, the following dimensionless variables are introduced:

$$\widetilde{x} = \frac{x}{\ell}, \quad \widetilde{t} = \frac{\kappa}{\rho c_e \ell^2} t, \quad \widetilde{u}_i = \frac{(\lambda + 2\mu)u_i}{\ell\gamma\theta_0}, \quad \widetilde{\sigma}_{ij} = \frac{\sigma_{ij}}{\gamma\theta_0}, \quad \widetilde{\theta} = \frac{\theta - \theta_0}{\theta_0},$$

where $\ell = \kappa/(\rho c_e c_s)$ is the dimensionless unit length and $c_s = \sqrt{(\lambda + 2\mu)/\rho}$ is the velocity of the longitudinal wave. Now, we define the coupling parameter

$$\delta_0 := \frac{\theta_0 \gamma^2}{\rho c_e (\lambda + 2\mu)}. \tag{8}$$

We will use this parameter to study the coupling effect of the governing equations. If we introduce the new Lamé constants

$$\widetilde{\mu} = \frac{\mu}{\lambda + 2\mu}, \quad \widetilde{\lambda} = \frac{\lambda}{\lambda + 2\mu},$$

then Eqs. (6) and (7), after dropping the tilde symbol for convenience, read as

$$\sigma_{ij,j} - \ddot{u}_i = 0, \tag{9}$$

$$\theta_{,ii} - \dot{\theta} - \delta_0 \dot{u}_{j,j} = 0, \tag{10}$$

where

$$\sigma_{ij} = 2\mu\varepsilon_{kl} + \lambda\varepsilon_{kk}\delta_{ij} - \theta\delta_{ij}. \tag{11}$$

The boundary conditions are assumed to be

$$\begin{aligned} u_i &= \overline{u}_i && \text{on } \Gamma_u \times [0, t_f], \\ t_i = \sigma_{ij} n_j &= \overline{t}_i && \text{on } \Gamma_t \times [0, t_f], \\ \theta &= \overline{\theta} && \text{on } \Gamma_\theta \times [0, t_f], \\ q = \theta_{,j} n_j &= \overline{q} && \text{on } \Gamma_q \times [0, t_f], \end{aligned}$$

where $\overline{u}_i, \overline{t}_i, \overline{\theta}$ and $\overline{q}$ are the prescribed displacement, traction, temperature and heat flux on the boundary Γ where $\Gamma = \Gamma_u \cup \Gamma_t$ and $\Gamma = \Gamma_\theta \cup \Gamma_q$. The vector $[n_1\ n_2] =: \boldsymbol{n}$ is the unit outward normal to the boundary Γ_t or Γ_q. The initial conditions are

$$\begin{aligned} u_i(x, 0) &= u_{i0}(x), \\ \dot{u}_i(x, 0) &= \dot{u}_{i0}(x), \\ \theta(x, 0) &= 0, \end{aligned}$$

for $x \in \Omega$, where u_{i0} and $\dot{u}_{i0}$ are initial displacement and initial velocity, respectively. Since in the dimensionless equations θ describes the *difference* (and not absolute) temperature, it should be zero at initial time $t = 0$.

4 Functionals from local weak forms

Suppose that $X = \{x_1, x_2, \ldots, x_N\}$ is a set of scattered meshless points in $\overline{\Omega}$. The same set X will be used for both trial and test point sets in our numerical simulation. Besides, the same points are used for approximating both displacement field and temperature function.

For both equations of motion and heat, instead of a global weak form over entire Ω, we use some local weak forms over small subdomains Ω_k around the test points $x_k \in \text{int}(\Omega)$.

Taking integration with respect to the spatial variable from both sides of Eq. (9) against some proper test functions v_i, $i = 1, 2$ (usually $v_1 = v_2 =: v$), and then applying the Gauss divergence theorem, the local weak forms

$$-\int_{\partial\Omega_k} v\sigma_{ij} n_j \mathrm{d}\Gamma + \int_{\Omega_k} \sigma_{ij} v_{,j} \mathrm{d}\Omega + \int_{\Omega_k} v\ddot{u}_i \,\mathrm{d}\Omega = 0 \tag{12}$$

are derived for $k = 1, 2, \ldots, N_I$, where N_I is the number of points inside Ω. Since we are going to perform a Petrov–Galerkin method, the test function v can be chosen from an arbitrary space independent of the trial space.

The natural and essential boundary conditions $u_i = \overline{u}_i$ and $t_i = \overline{t}_i$ will be imposed using a proper collocation method.

Now we define

$$L_k^{S_{\text{dp}}}(\boldsymbol{u}) := \int_{\Omega_k} \boldsymbol{\varepsilon}_v D\mathcal{L}\boldsymbol{u}\,\mathrm{d}\Omega - \int_{\partial\Omega_k} v\mathcal{N}D\mathcal{L}\boldsymbol{u}\,\mathrm{d}\Gamma,$$
$$L_k^{M_{\text{dp}}}(\boldsymbol{u}) := \int_{\Omega_k} v\boldsymbol{u}\,\mathrm{d}\Omega,$$
$$L_k^{K_{\text{tmp}}}(\theta) := -\int_{\Omega_k} \theta\nabla v\,\mathrm{d}\Omega + \int_{\partial\Omega_k} v\theta\boldsymbol{n}\,\mathrm{d}\Gamma,$$

where the subscripts "dp" and "tmp" stand for displacement and temperature functions, respectively. Using these definitions, (12) can be read as

$$L_k^{S_{\text{dp}}}(\boldsymbol{u}) + \frac{\partial^2}{\partial t^2} L_k^{M_{\text{dp}}}(\boldsymbol{u}) + L_k^{K_{\text{tmp}}}(\theta) = 0, \quad k = 1, 2, \ldots, N_I. \tag{13}$$

In the above formulation the displacement vector $[u_1\ u_2]^T$ is indicated by $\boldsymbol{u}$, and

$$\mathcal{L} = \begin{bmatrix} \frac{\partial}{\partial x} & 0 \\ 0 & \frac{\partial}{\partial y} \\ \frac{\partial}{\partial y} & \frac{\partial}{\partial x} \end{bmatrix},$$

and for a problem of isotropic material, the stress-strain matrix D is defined by

$$D = \begin{bmatrix} \lambda + 2\mu & \lambda & 0 \\ \lambda & \lambda + & 2\mu \quad 0 \\ 0 & 0 & \mu \end{bmatrix}.$$

Besides,

$$\mathcal{N} = \begin{bmatrix} n_1 & 0 & n_2 \\ 0 & n_2 & n_1 \end{bmatrix}, \quad \boldsymbol{n} = [n_1\ n_2]^T, \quad \boldsymbol{\varepsilon}_v = \begin{bmatrix} v_{,1} & 0 & v_{,2} \\ 0 & v_{,2} & v_{,1} \end{bmatrix}, \quad \nabla v = [v_{,1}\ v_{,2}]^T.$$

To enforce the displacement boundary condition $\boldsymbol{u} = \overline{\boldsymbol{u}}$ on Γ_u we define the functionals

$$L_k^{B_{\text{dp}}}(\boldsymbol{u}) := \delta_{x_k} \circ \boldsymbol{u}, \quad x_k \in \Gamma_u,$$

and to enforce the traction boundary condition $\boldsymbol{t} = \overline{\boldsymbol{t}}$ on Γ_t we define, according to (11), the following types of functionals:

$$L_k^{B_{\text{tru}}}(\boldsymbol{u}) := \delta_{x_k} \circ (\mathcal{N}D\mathcal{L}\boldsymbol{u}), \quad x_k \in \Gamma_t,$$
$$L_k^{B_{\text{trt}}}(\theta) := -\delta_{x_k} \circ (\theta\boldsymbol{n}), \quad x_k \in \Gamma_t,$$

where the superscripts B_{dp} and B_{tr} stand for displacement and traction boundary conditions. The latter has been decomposed to B_{tru} and B_{trt}. Consequently, the boundary conditions define the following functional equations:

$$L_k^{B_{\text{dp}}}(\boldsymbol{u}) := \overline{\boldsymbol{u}}(x_k), \quad x_k \in \Gamma_u, \tag{14}$$
$$L_k^{B_{\text{tru}}}(\boldsymbol{u}) + L_k^{B_{\text{trt}}}(\theta) := \overline{\boldsymbol{t}}(x_k), \quad x_k \in \Gamma_t. \tag{15}$$

Similarly, the local weak forms of the heat equation (10) can be written as

$$-\int_{\partial\Omega_k} v\theta_{,j} n_j \mathrm{d}\Gamma + \int_{\Omega_k} \theta_{,j} v_{,j} \mathrm{d}\Omega + \int_{\Omega_k} v\dot{\theta}\,\mathrm{d}\Omega + \delta_0 \int_{\Omega_k} v\dot{u}_{j,j}\,\mathrm{d}\Omega = 0 \tag{16}$$

for $k = 1, 2, \ldots, N_I$. To write these equations and the corresponding boundary conditions in an abstract functional form, we define

$$L_k^{S_{\text{tmp}}}(\theta) := \int_{\Omega_k} \nabla\theta \cdot \nabla v\,\mathrm{d}\Omega - \int_{\partial\Omega_k} \nabla\theta \cdot \boldsymbol{n}\, v\,\mathrm{d}\Gamma,$$

$$
\begin{aligned}
L_k^{M_{\text{tmp}}}(\theta) &:= \int_{\Omega_k} \theta v \, \mathrm{d}\Omega, \\
L_k^{C_{\text{dp}}}(\boldsymbol{u}) &:= \delta_0 \int_{\Omega_k} \operatorname{div}(\boldsymbol{u}) v \, \mathrm{d}\Omega, \\
L_k^{B_{\text{tmp}}}(\theta) &:= \delta_{x_k} \circ \theta, \\
L_k^{B_{\text{flx}}}(\theta) &:= \delta_{x_k} \circ (\nabla\theta \cdot \boldsymbol{n}).
\end{aligned}
$$

Thus we have

$$
L_k^{S_{\text{tmp}}}(\theta) + \frac{\partial}{\partial t} L_k^{M_{\text{tmp}}}(\theta) + \frac{\partial}{\partial t} L_k^{C_{\text{dp}}}(\boldsymbol{u}) = 0, \quad k = 1, 2, \ldots, N_I, \tag{17}
$$

for the internal points, and

$$
L_k^{B_{\text{tmp}}}(\theta) := \overline{\theta}(x_k), \quad x_k \in \Gamma_\theta, \tag{18}
$$

$$
L_k^{B_{\text{flx}}}(\theta) := \overline{q}(x_k), \quad x_k \in \Gamma_q, \tag{19}
$$

for the boundary points. In the next section, we will discuss the application of the GMLS approximation to the semi-discrete functional equations (13)–(15) and (17)–(19) to convert them to a full-discrete linear system of coupled equations.

5 DMLPG method and time integration scheme

All linear functionals L_k (ignoring the superscripts) of the previous section can be directly and stably approximated by the GMLS approximation of Sect. 2. We categorize these functionals in four groups as below:

(1): $L_k^{S_{\text{dp}}}$, $L_k^{M_{\text{dp}}}$, $L_k^{B_{\text{dp}}}$ and $L_k^{B_{\text{tru}}}$,
(2): $L_k^{S_{\text{tmp}}}$, $L_k^{M_{\text{tmp}}}$, $L_k^{B_{\text{tmp}}}$ and $L_k^{B_{\text{flx}}}$,
(3): $L_k^{K_{\text{tmp}}}$ and $L_k^{B_{\text{trt}}}$,
(4): $L_k^{C_{\text{dp}}}$.

For functionals of group (1), the GMLS approximation gives

$$
L_k(\boldsymbol{u}) \approx \widehat{L}_k(\boldsymbol{u}) = \sum_{j=1}^{N} A_{kj} \boldsymbol{u}(x_j, t),
$$

where A_{kj} is a 2×2 matrix depending on functional L_k and trial point x_j via indices k and j, respectively. Let A be a $2N_I \times 2N$ matrix with block elements A_{kj} for $k = 1, \ldots, N_I$ and $j = 1, 2, \ldots, N$. According to (5) if $A_{k,:}$ represents the k-th block row of A, then

$$
A_{k,:} = L_k(\boldsymbol{p}) B \in \mathbb{R}^{2 \times 2N},
$$

where $B \in \mathbb{R}^{2Q \times 2N}$ is a block matrix with

$$
B_{ij} = \begin{bmatrix} \widetilde{B}_{ij} & 0 \\ 0 & \widetilde{B}_{ij} \end{bmatrix} \in \mathbb{R}^{2 \times 2}, \quad \text{where} \quad \widetilde{B} := (P^T W P)^{-1} W P^T \in \mathbb{R}^{Q \times N}. \tag{20}
$$

The matrices P and W are defined in Sect. 2, and here $\boldsymbol{p}$ is defined by

$$
\boldsymbol{p} = \begin{bmatrix} p_1(x) & p_2(x) & \cdots & p_Q(x) \\ p_1(x) & p_2(x) & \cdots & p_Q(x) \end{bmatrix} \in \mathbb{R}^{2 \times Q}, \tag{21}
$$

and thus $L_k(\boldsymbol{p}) \in \mathbb{R}^{2 \times 2Q}$. The rows of $\boldsymbol{p}$ are the same because we use the same approximation space for both u_1 and u_2. We can easily establish that

$$
L_k^{B_{\text{dp}}}(\boldsymbol{p}) = \big[\Pi_1(x), \Pi_2(x), \ldots, \Pi_Q(x)\big] \in \mathbb{R}^{2 \times 2Q},
$$

where

$$\Pi_j(x) := \begin{bmatrix} p_j(x) & 0 \\ 0 & p_j(x) \end{bmatrix}, \quad j = 1, 2, \ldots, Q. \tag{22}$$

Similarly,

$$L_k^{M_{\rm dp}}(\boldsymbol{p}) = \Big[\underbrace{\int_{\Omega_k} v\Pi_1(x)\mathrm{d}\Omega}_{\in\mathbb{R}^{2\times 2}}, \underbrace{\int_{\Omega_k} v\Pi_2(x)\mathrm{d}\Omega}_{\in\mathbb{R}^{2\times 2}}, \ldots, \underbrace{\int_{\Omega_k} v\Pi_Q(x)\mathrm{d}\Omega}_{\in\mathbb{R}^{2\times 2}} \Big] \in \mathbb{R}^{2\times 2Q}.$$

For functionals $L_k^{B_{\rm tru}}$ we have

$$L_k^{B_{\rm tru}}(\boldsymbol{p}) = \Big[\underbrace{\mathcal{N}D\Pi_1}_{\in\mathbb{R}^{2\times 2}}, \underbrace{\mathcal{N}D\Pi_2}_{\in\mathbb{R}^{2\times 2}}, \ldots, \underbrace{\mathcal{N}D\Pi_Q}_{\in\mathbb{R}^{2\times 2}} \Big] \in \mathbb{R}^{2\times 2Q},$$

with a new definition for Π_j as below:

$$\Pi_j := \Pi_j(x) = \mathcal{L}\begin{bmatrix} p_j(x) \\ p_j(x) \end{bmatrix} = \begin{bmatrix} p_{j,1}(x) & 0 \\ 0 & p_{j,2}(x) \\ p_{j,2}(x) & p_{j,1}(x) \end{bmatrix}, \quad j = 1, 2, \ldots, Q. \tag{23}$$

Similarly, for $L_k^{S_{\rm dp}}$ we can obtain

$$\begin{aligned} L_k^{S_{\rm dp}}(\boldsymbol{p}) = &\Big[\int_{\Omega_k} \boldsymbol{\varepsilon}_v D\Pi_1 \mathrm{d}\Omega, \int_{\Omega_k} \boldsymbol{\varepsilon}_v D\Pi_2 \mathrm{d}\Omega, \ldots, \int_{\Omega_k} \boldsymbol{\varepsilon}_v D\Pi_Q \mathrm{d}\Omega \Big] \\ &- \Big[\int_{\partial\Omega_k} v\mathcal{N}D\Pi_1 \mathrm{d}\Gamma, \int_{\partial\Omega_k} v\mathcal{N}D\Pi_2 \mathrm{d}\Gamma, \ldots, \int_{\partial\Omega_k} v\mathcal{N}D\Pi_Q \mathrm{d}\Gamma \Big] \in \mathbb{R}^{2\times 2Q}, \end{aligned}$$

where Π_j are defined by (23).

To distinguish between the notations, the matrices $S_{\rm dp}$, $M_{\rm dp}$, $B_{\rm dp}$ and $B_{\rm tru}$ will be used instead GMLS matrix A for functionals $L_k^{S_{\rm dp}}$, $L_k^{M_{\rm dp}}$, $L_k^{B_{\rm dp}}$ and $L_k^{B_{\rm tru}}$, respectively. The size of both $S_{\rm dp}$ and $M_{\rm dp}$ is $2N_I \times 2N$ where N_I is the number of internal test points. The sizes of $B_{\rm dp}$ and $B_{\rm tr}$ are $2N_u \times 2N$ and $2N_t \times 2N$, respectively, where N_u and N_t are the numbers of test points on boundaries Γ_u and Γ_t, respectively.

For functionals of group (2), the GMLS directly approximates $L_k(\theta)$ by

$$L_k(\theta) \approx \widehat{L}_k(\theta) = \sum_{j=1}^{N} a_{kj}\theta(x_j, t),$$

where according to (5) we have

$$\boldsymbol{a}_{k,:} = L_k(\boldsymbol{p})B \in \mathbb{R}^{1\times N},$$

where $\boldsymbol{p} = [p_1, \ldots, p_Q]$ and $B = (P^T W P)^{-1} W P^T \in \mathbb{R}^{Q\times N}$. It remains to formulate $L_k(\boldsymbol{p})$ for this class of functionals. One can easily show that

$$\begin{aligned} L_k^{B_{\rm tmp}}(\boldsymbol{p}) &= \boldsymbol{p}(x_k) = \Big[p_1(x_k), p_2(x_k), \ldots, p_Q(x_k) \Big] \in \mathbb{R}^{1\times Q}, \\ L_k^{B_{\rm flx}}(\boldsymbol{p}) &= \Big[\nabla p_1(x_k)\cdot\boldsymbol{n}(x_k), \ldots, \nabla p_Q(x_k)\cdot\boldsymbol{n}(x_k) \Big] \in \mathbb{R}^{1\times Q}, \\ L_k^{M_{\rm tmp}}(\boldsymbol{p}) &= \Big[\int_{\Omega_k} vp_1(x)\mathrm{d}\Omega, \int_{\Omega_k} vp_2(x)\mathrm{d}\Omega, \ldots, \int_{\Omega_k} vp_Q(x)\mathrm{d}\Omega \Big] \in \mathbb{R}^{1\times Q}, \\ L_k^{S_{\rm tmp}}(\boldsymbol{p}) &= \Big[\int_{\Omega_k} \nabla p_1 \cdot \nabla v \,\mathrm{d}\Omega, \ldots, \int_{\Omega_k} \nabla p_Q \cdot \nabla v \,\mathrm{d}\Omega \Big] \\ &\quad - \Big[\int_{\partial\Omega_k} v\nabla p_1 \cdot \boldsymbol{n}\,\mathrm{d}\Gamma, \ldots, \int_{\partial\Omega_k} v\nabla p_Q \cdot \boldsymbol{n}\,\mathrm{d}\Gamma \Big] \in \mathbb{R}^{1\times Q}. \end{aligned}$$

To form the final linear system of equations we use $S_{\text{tmp}} \in \mathbb{R}^{N_I \times N}$, $M_{\text{tmp}} \in \mathbb{R}^{N_I \times N}$, $B_{\text{tmp}} \in \mathbb{R}^{N_\theta \times N}$ and $B_{\text{flx}} \in \mathbb{R}^{N_q \times N}$ instead of the GMLS matrix A. Here N_θ and N_q are the numbers of points on Γ_θ and Γ_q, respectively.

For functionals of group (3) we write the GMLS approximation as

$$L_k(\theta) \approx \widehat{L}_k(\theta) = \sum_{j=1}^{N} A_{kj}\theta(x_j, t),$$

where A_{kj} are 2×1 matrices for all k and j. If $A = (A_{kj})$ then the k-th block row of A is

$$A_{k,:} = L_k(\boldsymbol{p})B \in \mathbb{R}^{2\times N},$$

where $\boldsymbol{p} = [p_1, \ldots, p_Q]$, $B = (P^T W P)^{-1} W P^T \in \mathbb{R}^{Q\times N}$ and

$$\begin{aligned} L_k^{K_{\text{tmp}}}(\boldsymbol{p}) = &-\Big[\underbrace{\int_{\Omega_k} p_1 \nabla v \,\mathrm{d}\Omega}_{\in\mathbb{R}^{2\times 1}}, \ldots, \underbrace{\int_{\Omega_k} p_Q \nabla v \,\mathrm{d}\Omega}_{\in\mathbb{R}^{2\times 1}}\Big] \\ &+ \Big[\underbrace{\int_{\partial\Omega_k} v p_1 \boldsymbol{n} \,\mathrm{d}\Gamma}_{\in\mathbb{R}^{2\times 1}}, \ldots, \underbrace{\int_{\partial\Omega_k} v p_Q \boldsymbol{n} \,\mathrm{d}\Gamma}_{\in\mathbb{R}^{2\times 1}}\Big] \in \mathbb{R}^{2\times Q}, \\ L_k^{B_{\text{trt}}}(\boldsymbol{p}) = &-\Big[\underbrace{p_1\boldsymbol{n}}_{\in\mathbb{R}^{2\times 1}}, \ldots, \underbrace{p_Q\boldsymbol{n}}_{\in\mathbb{R}^{2\times 1}}\Big] \in \mathbb{R}^{2\times Q}. \end{aligned}$$

The notations K_{tmp} and B_{trt} will be used instead of A. The size of both matrices is $2N_I \times N$.

Finally, for functionals of group (4) the GMLS approximation can be written as

$$L_k(\boldsymbol{u}) \approx \widehat{L}_k(\boldsymbol{u}) = \sum_{j=1}^{N} A_{kj}\boldsymbol{u}(x_j, t),$$

where A_{kj} are 1×2 matrices for all k and j. If $A = (A_{kj})$ then the k-th row of A is

$$A_{k,:} = L_k(\boldsymbol{p})B \in \mathbb{R}^{1\times 2N},$$

where $\boldsymbol{p}$ is defined by (21), $B \in \mathbb{R}^{Q\times 2N}$ is formed via (20) and

$$L_k^{C_{\text{dp}}}(\boldsymbol{p}) = \delta_0\Big[\underbrace{\int_{\Omega_k} v\nabla p_1 \,\mathrm{d}\Omega}_{\in\mathbb{R}^{1\times 2}}, \ldots, \underbrace{\int_{\Omega_k} v\nabla p_Q \,\mathrm{d}\Omega}_{\in\mathbb{R}^{1\times 2}}\Big] \in \mathbb{R}^{1\times 2Q},$$

where δ_0 is the coupling parameter. At the end the notation C_{dp} is used instead of A. The size of this matrix is $N_I \times 2N$.

To form the final differential algebraic equations, we define the vector $U(t)$ by

$$U(t) := \big[u_1(x_1, t), u_2(x_1, t), \ldots, u_1(x_N, t), u_2(x_N, t), \theta(x_1, t), \ldots, \theta(x_N, t)\big]^T \in \mathbb{R}^{3N\times 1}$$

and the matrices M, C and S, all of size $3N \times 3N$, by

$$M = \left[\begin{array}{cc} M_{\text{dp}} & 0 \\ 0 & 0 \\ 0 & 0 \\ \hline 0 & 0 \\ 0 & 0 \\ 0 & 0 \end{array}\right], \quad C = \left[\begin{array}{cc} 0 & 0 \\ 0 & 0 \\ 0 & 0 \\ \hline C_{\text{dp}} & M_{\text{tmp}} \\ 0 & 0 \\ 0 & 0 \end{array}\right], \quad S = \left[\begin{array}{cc} S_{\text{dp}} & K_{\text{tmp}} \\ B_{\text{dp}} & 0 \\ B_{\text{tru}} & B_{\text{trt}} \\ \hline 0 & S_{\text{tmp}} \\ 0 & B_{\text{tmp}} \\ 0 & B_{\text{flx}} \end{array}\right],$$

Table 1 The CPU time used (sec.) for Example 6.1

Method	MLPG1	MLPG5	DMLPG1	DMLPG5
Run time	83	37	0.5	0.5

and the right-hand side vector $F(t)$ by

$$F(t) = \big[\underbrace{0, 0, \ldots, 0}_{2N_I \text{ times}}, \underbrace{\overline{\boldsymbol{u}}(x_1^u), \ldots, \overline{\boldsymbol{u}}(x_{N_u}^u)}_{2N_u \text{ times}}, \underbrace{\overline{\boldsymbol{t}}(x_1^t), \ldots, \overline{\boldsymbol{t}}(x_{N_t}^t)}_{2N_t \text{ times}},$$
$$\underbrace{0, 0, \ldots, 0}_{N_I \text{ times}}, \underbrace{\overline{\theta}(x_1^\theta), \ldots, \overline{\theta}(x_{N_\theta}^\theta)}_{N_\theta \text{ times}}, \underbrace{\overline{q}(x_1^q), \ldots, \overline{q}(x_{N_q}^q)}_{N_q \text{ times}}\big],$$

where N_I is the number of internal test points from X, and N_u, N_t, N_θ and N_q are the numbers of boundary test points on Γ_u, Γ_t, Γ_θ and Γ_q, respectively. The superscripts on the boundary points x_k denote the type of boundary in which the points x_k belong to that.

According to the above notation, the full-discrete final linear time-dependent system of equations can be written as

$$M\ddot{U}(t) + C\dot{U}(t) + SU(t) = F(t), \quad 0 < t \leqslant t_f. \tag{24}$$

This equation can be solved by any suitable time integration scheme. In this paper we apply the Newmark method [9]. The algorithm can be found in [14] and thus we omit the details here and refer the reader to the mentioned references.

As is clear from the construction process in this section, in DMLPG numerical integration is done over low-degree and close-form multi-dimensional polynomials. This is in contrast with the original MLPG method where one should integrate against nonclose-form and complicated MLS shape functions. This property reduces the computational cost of DMLPG remarkably. But it is not the whole story. If in addition the shifted polynomial basis functions are employed and if the same test function v is used for all local subdomains, then $L_k(\boldsymbol{p}) = L_j(\boldsymbol{p})$ provided that $\Omega_k = x + \Omega_j = \{x + y : y \in \Omega_j\}$, $x \in \mathbb{R}^2$. For example, for all interior test points the only one integral should be computed if all interior local subdomains have the same shape. This property reduces the cost of DMLPG in order of the cost of a MLS collocation method. This means that in DMLPG the numerical integration imposes no additional cost.

The computational costs of DMLPG and finite elements method (FEM) are also comparable. In both methods numerical integration is done over low-degree polynomial basis functions. In additions, both methods lead to sparse final linear systems.

Finally, we note that in this paper two kinds of test function v will be applied. If v is vanishing on $\partial\Omega_k$ then the first integrals in (12) and (16) vanish. In the MLPG literature, this technique is labeled as MLPG1. If v is chosen to be the characteristic function of the set Ω_k then the second integrals in (12) and (16) vanish and the resulting method is called MLPG5. The same labels can be used for DMLPG as well.

6 Numerical results

In this section two examples are presented to demonstrate the efficiency and accuracy of the proposed method. In both examples the shifted and scaled quadratic polynomial basis function and a Gaussian weight function are used. A 15-point Gauss-Legendre quadrature is employed for numerical integration in each axis of transferred local subdomains. The size of the supports of the GMLS approximation for all test points is assumed to be $3h$, where h is the fill distance of the trial points. We use an implicit and unconditionally stable average acceleration scheme (a Newmark time integration scheme; see Table 1 of [14]) to discretize the time domain. The time step $\Delta t = 0.05$ is used in all test examples. The problems are solved in dimensionless form and thus all involved parameters and variables are dimensionless.

The programs are written in MATLAB© and run on a Personal PC with 8 GB of RAM and a CPU with 4 physical/ 8 logical cores and 2.4 GHz processor speed.

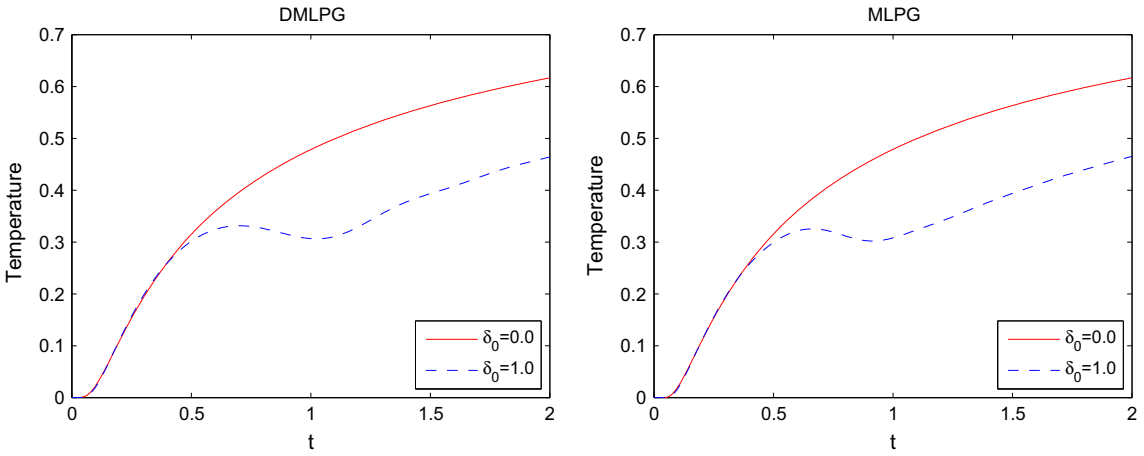

Fig. 1 The time history of temperature θ at $x = 1$ for uncoupled and coupled problems

6.1 Example 1

A half space ($x > 0$) subjected to thermal heating at $x = 0$, by sudden exposure to a unit temperature at time $t = 0^+$, which remains constant thereafter is considered for the first example. The half space is modeled by a plate of length 5 and hight 1 (dimensionless length) and 49×9 regular meshless points are used to discretize the plate. The problem is essentially one-dimensional and thus u_2 can be assumed to be zero on all sides of the plate. Traction-free boundary conditions are assumed on the remaining parts. The plate is thermally insulated at the three other edges. The plate material is taken as stainless steel with the properties

$$\begin{aligned} \nu &= 0.25, \\ E &= 2 \times 10^7 \text{ kg/cm}^2, \\ \gamma &= 3.34 \times 10^4 \text{ kg/°K/cm/s}^2, \\ \lambda + 2\mu &= 1.99 \times 10^9 \text{ kg/cm/s}^2, \\ \rho &= 7.82 \times 10^{-3} \text{ kg/cm}^3, \\ c &= 4.61 \times 10^6 \text{ cm}^2/\text{°K/s}^2, \\ \kappa &= 1.70 \times 10^3 \text{ kg} \times \text{cm/°K/s}^3. \end{aligned}$$

Note that in the dimensionless form the only independent required values are E and ν. The approximate solutions of this problem have been obtained by using the finite element method (FEM) [19,29] and the boundary element method (BEM) [6,10,30]. We compare the results of the MLPG and DMLPG methods. Our results are obtained for time history on a particular dimensionless location $x = 1$. This point is the location of the elastic wave front at the dimensionless time $t = 1$. The time evolutions of temperature θ, displacement u_1 and stress σ_{11} for $\delta_0 = 0$ (uncoupled problem) and $\delta_0 = 1$ (coupled problem) are presented and compared in Figs. 1, 2 and 3 at point $x = 1$ for $t \in [0, 2]$. As we can see from Fig. 1, the temperature distribution of the coupled problem behind the wave front asymptotically approaches the uncoupled solution with increasing time. The effect of coupling is to accelerate thermal diffusion ahead of the wave front. Our results show that a negative temperature gradient is generated ahead of the wave front for the coupled problem because the temperature plot is not thence monotone. Sudden change in displacement at the wave front is associated with the arrival of the elastic and thermal waves. This phenomenon also appears in Fig. 3 for the stress plot.

The results of MLPG and DMLPG are approximately the same except for σ_{11} in Fig. 3 where the DMLPG solution produces a little more oscillation after time $t = 1$. They are in acceptable agreement with those given in [6,10,19] with FEM and BEM. Note that the analytical solution for the coupled problem is not available.

As we pointed out, the computational cost of DMLPG is remarkably less than MLPG. For this example the run times are reported in Table 1. A comparison between the run times for constructing the final stiffness and mass matrices is also provided in Fig. 4 for different numbers of trial meshless points. The differences

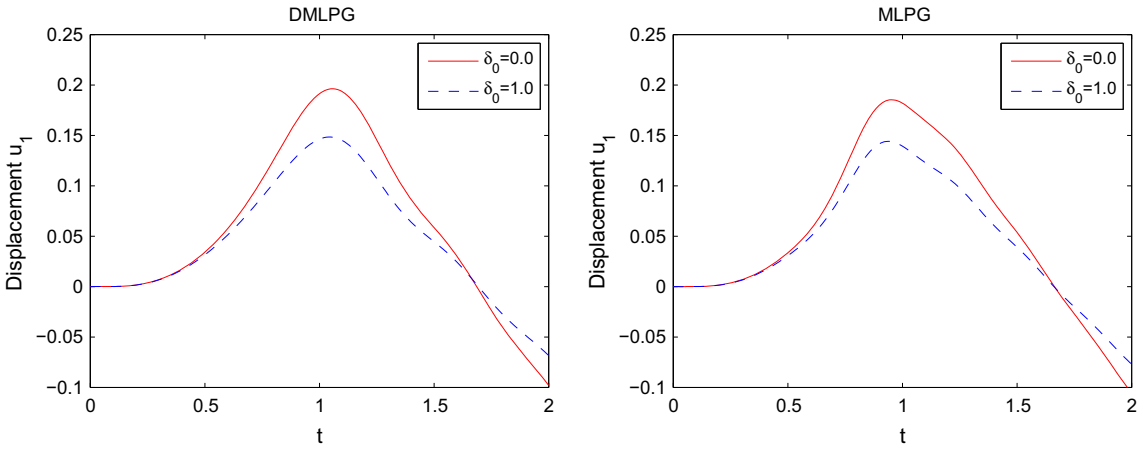

Fig. 2 The time history of displacement u_1 at $x = 1$ for uncoupled and coupled problems

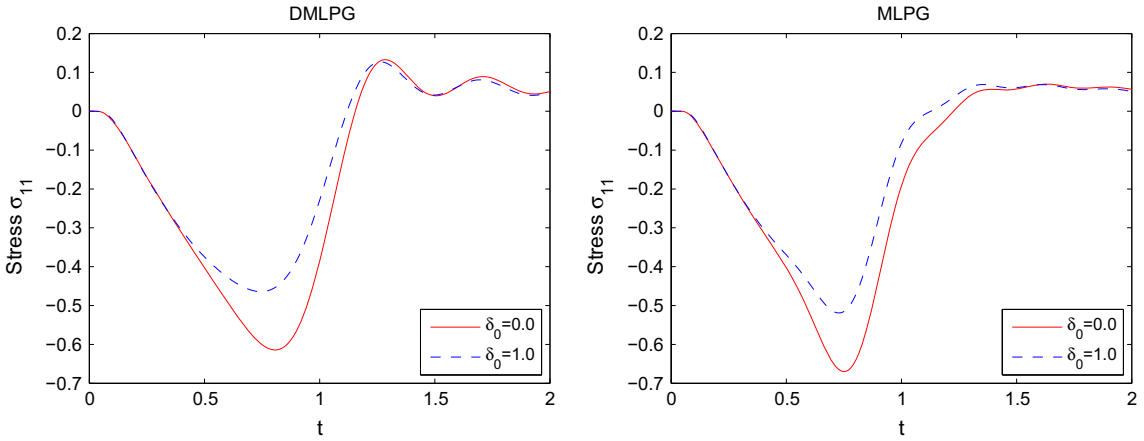

Fig. 3 The time history of stress σ_{11} at $x = 1$ for uncoupled and coupled problems

between the costs of the DMLPG and MLPG methods are large enough to convince us to replace the original MLPG by the new DMLPG for many engineering problems.

6.2 Example 2

Consider a square plate of isotropic and homogeneous material. The dimensionless plate is assumed to be the square $[0, 10] \times [-5, 5]$ and 21×21 regular meshless points are used. The Young's modulus E and Poisson's ratio ν are assumed to be 1 and 0.3, respectively. The boundary conditions on the top and bottom sides of the plate are $t_1 = t_2 = 0$ and $q = 0$. On the right side we prescribe $u_1 = u_2 = 0$ and $q = 0$. Three types of boundary conditions are imposed on the edge $x = 0$ (the left side):

(1) The thermal shock $\theta(t) = f(t)$, and $t_1 = 0 = t_2 = 0$,
(2) The pressure shock $t_1(t) = f(t)$, and $t_2 = 0$ and $q = 0$, and finally
(3) Combination of thermal and pressure shocks $\theta(t) = f(t)$ and $t_1(t) = f(t)$, $t_2 = 0$,

where

$$f(t) = 5t \exp(-2t), \quad t > 0.$$

Such a problem is numerically solved using BEM in [10] and MLPG with Kriging interpolants in [33].

Again MLPG and DMLPG results are compared in Figs. 5, 6, 7, 8, 9, 10, 11, 12, 13. In all three cases the comparison of the temperature θ, axial displacement u_1, and the axial stress σ_{11} along the x-axis at

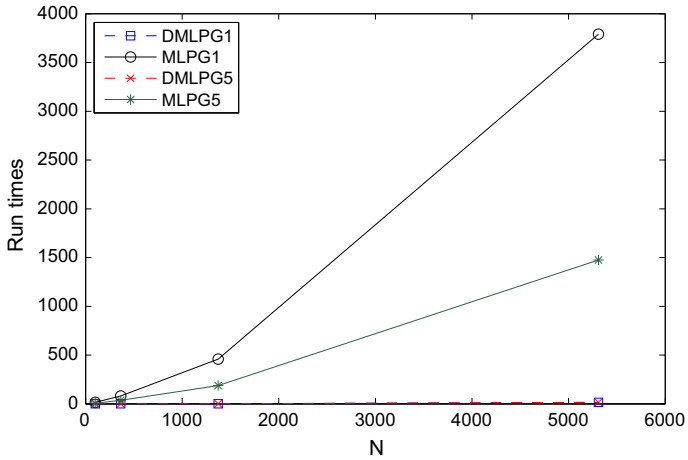

Fig. 4 Comparing the CPU times (sec.) used in MLPG and DMLPG methods

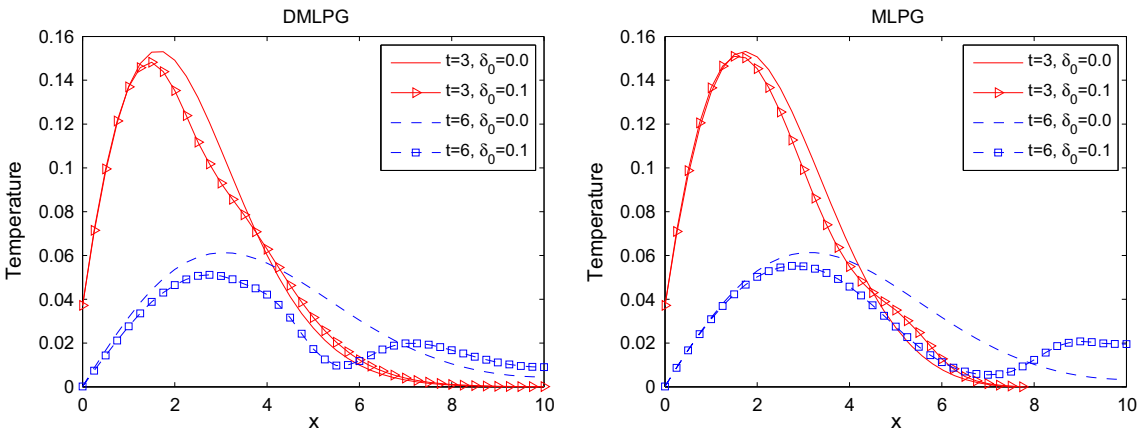

Fig. 5 Comparison of the dimensionless temperature at the middle line of the plate for temperature loading

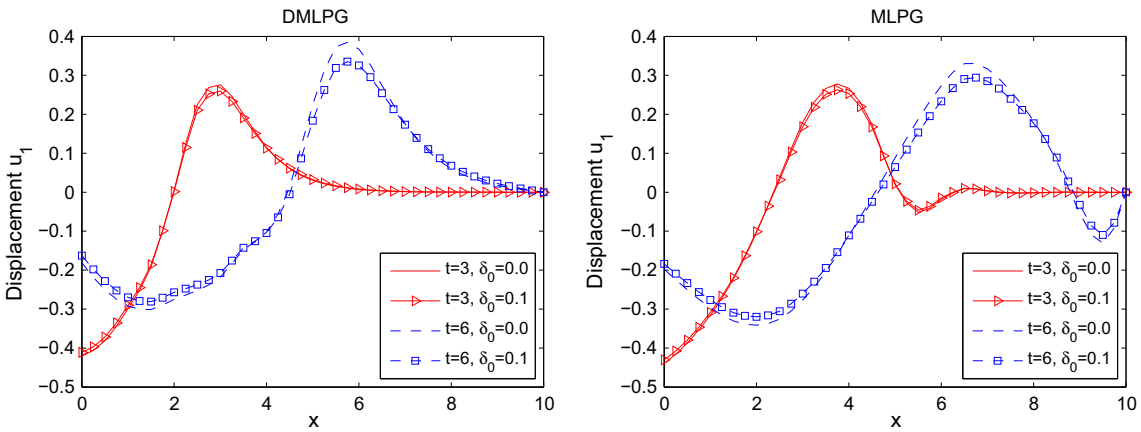

Fig. 6 Comparison of the dimensionless axial displacement at middle line of the plate for temperature loading

dimensionless times $t = 3$ and $t = 6$ are obtained for both uncoupled ($\delta_0 = 0$) and coupled ($\delta_0 = 0.1$) problems. Due to the coupling effect, the temperature distribution of the uncoupled and coupled cases are significantly different. For problem (2) the temperature is identically zero for the uncoupled case because we are solving a homogenous heat equation with zero boundary conditions. However, in the coupled case the

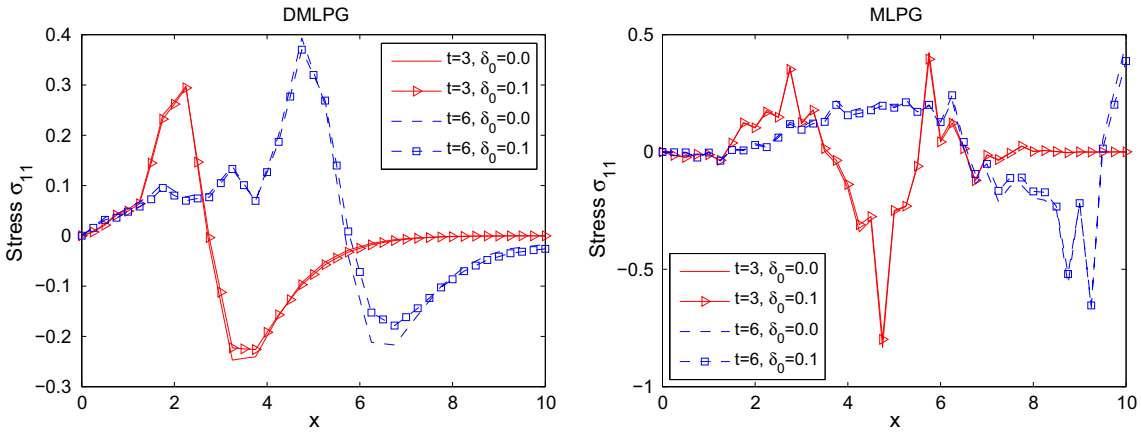

Fig. 7 Comparison of the dimensionless axial stress at middle line of the plate for temperature loading

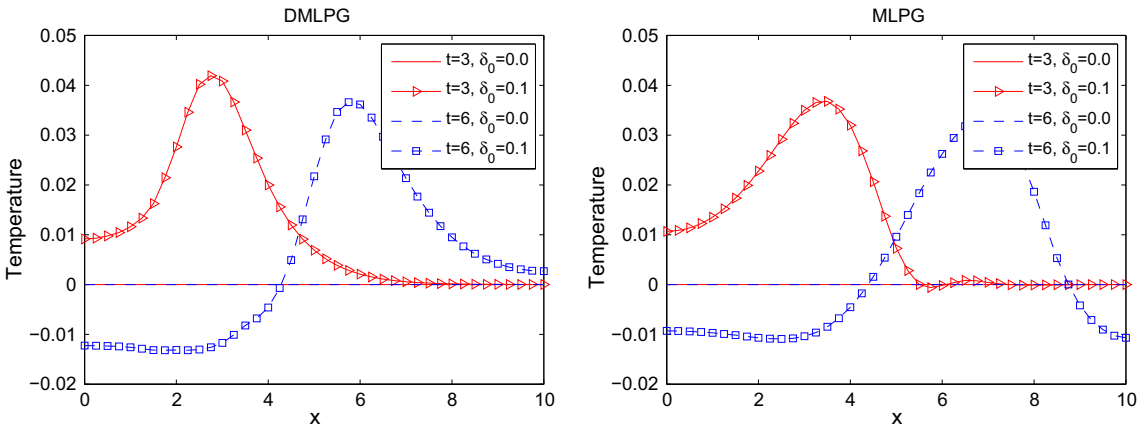

Fig. 8 Comparison of the dimensionless temperature at middle line of the plate for traction loading

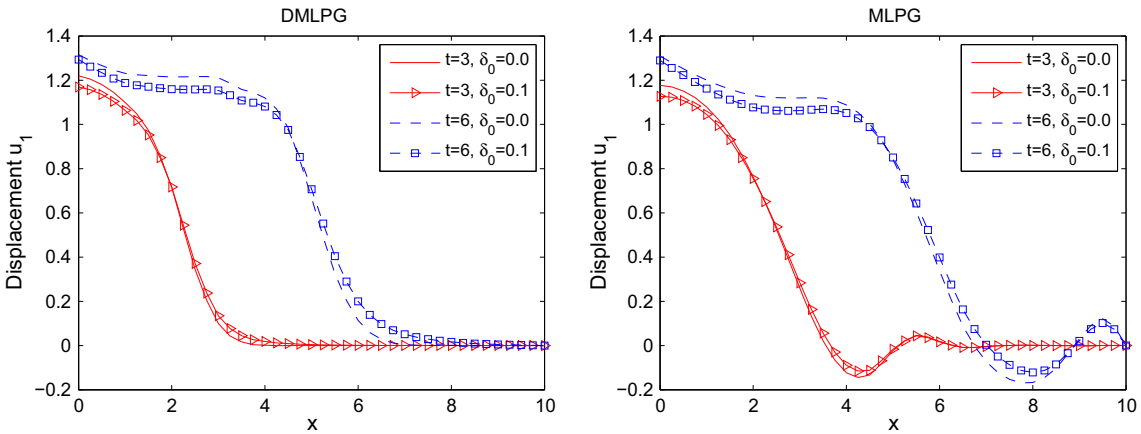

Fig. 9 Comparison of the dimensionless axial displacement at middle line of the plate for traction loading

temperature rises due to the fact that the mechanical energy induced by the pressure shock being changed into the heat energy. The displacement and stress distributions have smaller changes for coupled and uncoupled problems in all cases. These results of DMLPG are in good agreement with those given in [10,33]. However MLPG produces poor stress solutions in all cases.

The CPU run times are reported in Table 2. DMLPG is dramatically faster than MLPG.

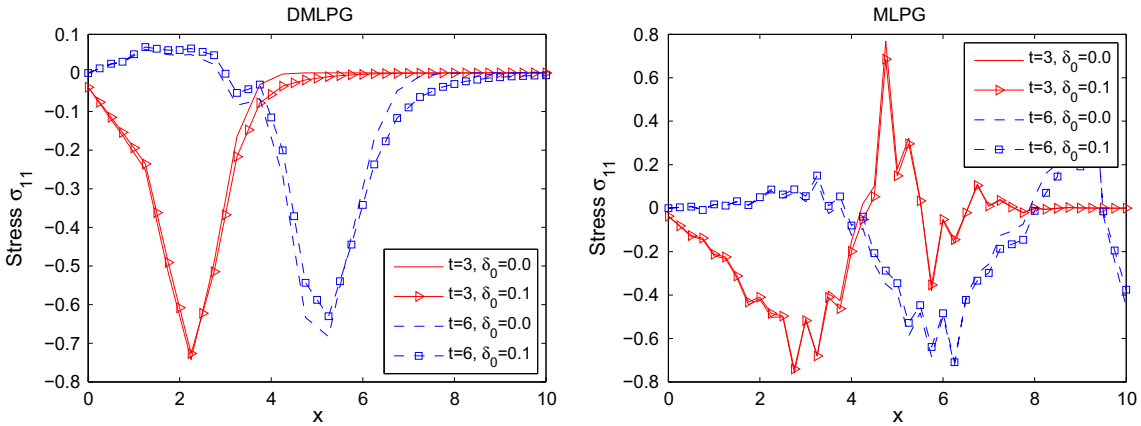

Fig. 10 Comparison of the dimensionless axial stress at middle line of the plate for traction loading

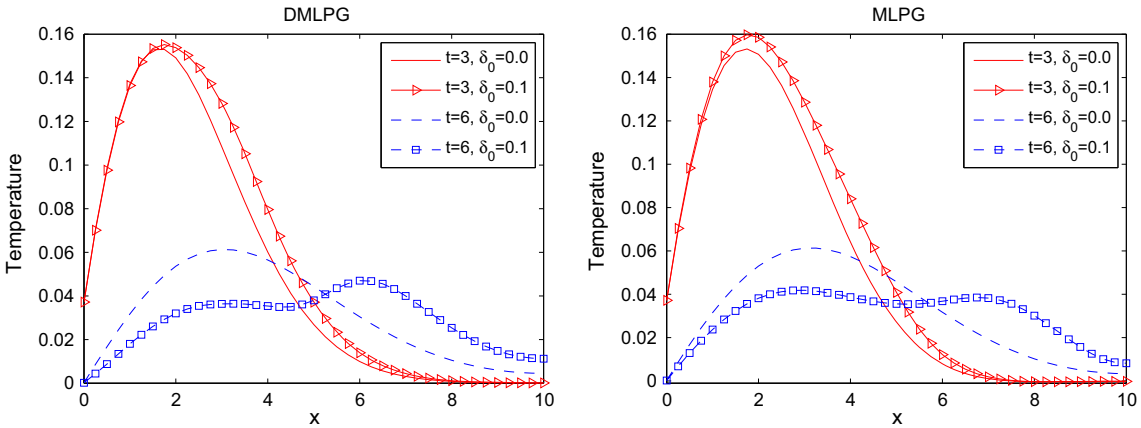

Fig. 11 Comparison of the dimensionless temperature at middle line of the plate for temperature and traction loadings

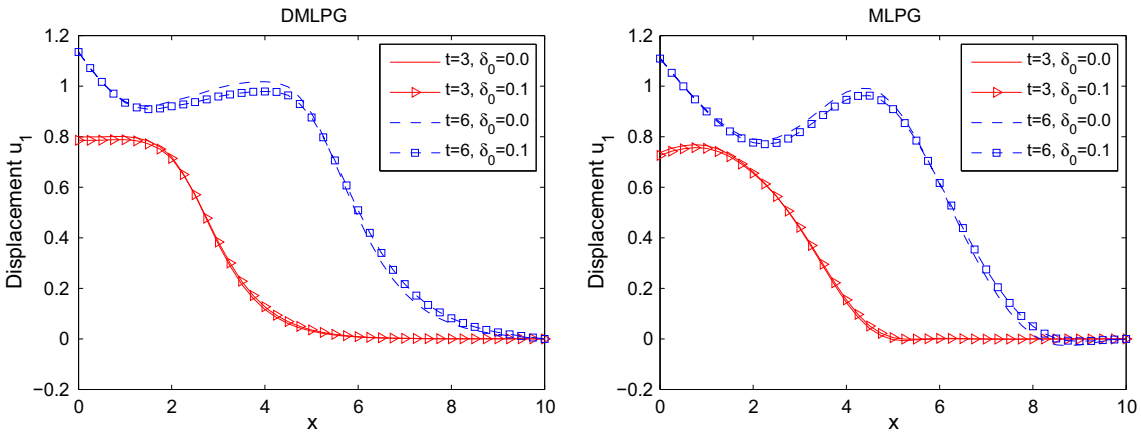

Fig. 12 Comparison of the dimensionless axial displacement at middle line of the plate for temperature and traction loadings

7 Conclusion

In this paper the direct meshless local Petrov–Galerkin (DMLPG) method has been applied for numerical solution of the coupled thermoelastic problem. The governing equations have been first converted to a dimensionless form and then the generalized moving least square approximation has been employed to directly approximate the local weak forms of coupled displacement and temperature equations from scattered data

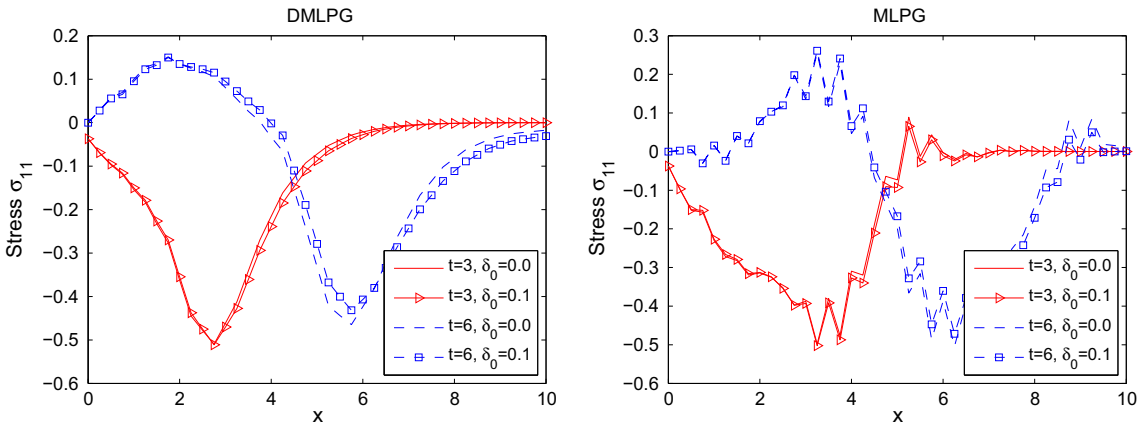

Fig. 13 Comparison of the dimensionless axial stress at middle line of the plate for temperature and traction loadings

Table 2 The CPU time used (sec.) for Example 6.2

Method	MLPG1	MLPG5	DMLPG1	DMLPG5
Run time	113	50	0.6	0.6

point layouts. The Newmark time integration method has been used to discretize the time domain. The method has been explained and computationally verified to be much faster than the original MLPG method. Finally, we note that the smooth approximant functions of both MLPG and DMLPG methods need to be modified in order to capture the discontinuous properties in thermoelastic waves produced by a delta force [31]. We do not pursue this here and leave it for a future work.

References

1. Apostolakis, G., Dargush, G.F.: Variational methods in irreversible thermoelasticity: theoretical developments and minimum principles for the discrete form. Acta Mech. **224**, 2065–2088 (2013)
2. Atluri, S.N., Shen, S.: The Meshless Local Petrov–Galerkin (MLPG) Method. Tech Science Press, Encino (2002)
3. Belytschko, T., Krongauz, Y., Organ, D., Fleming, M., Krysl, P.: Meshless methods: an overview and recent developments. Comput. Methods Appl. Mech. Eng. **139**, 3–47 (1996)
4. Bobaru, F., Mukhrejee, S.: Meshless approach to shape optimization of linear thermoelastic solids. Int. J. Numer. Methods Eng. **53**, 765–796 (2003)
5. Carter, J.P., Booker, J.R.: Finite element analysis of coupled thermoelasticity. Comput. Struct. **31**, 73–80 (1989)
6. Chen, J., Dargush, G.F.: BEM for dynamic proelastic and thermoelastic analysis. Int. J. Solids Struct. **32**, 2257–2278 (1995)
7. Ching, H.K., Yen, S.C.: Transient thermoelastic deformations of 2-D functionally graded beams under nonuniformly convective heat supply. Compos. Struct. **73**, 381–393 (2006)
8. Hetnarski, R.B., Eslami, M.R.: Thermal Stresses: Advanced Theory and Applications. Springer, Berlin (2009)
9. Hoghes, T., Pister, K., Taylor, R.: Implicit-explicit finite elements in nonlinear transient analysis. Comput. Methods Appl. Mech. Eng. **17–18, Part 1**, 159–182 (1979)
10. Hosseini-Tehrani, P., Eslami, M.R.: BEM analysis of thermal and mechanical shock in a two-dimensional finite domain considering coupled thermoelasticity. Eng. Anal. Bound. Elem. **24**, 249–257 (2000)
11. Jabbari, M., Eslami, M., Dehbani, H.: An exact solution for classic coupled thermoelasticity in spherical coordinates. J. Press. Vessel Technol. **31**, 31201–31211 (2010)
12. Jabbari, M., Eslami, M., Dehbani, H.: An exact solution for classic coupled thermoelasticity in cylindrical coordinates. J. Press. Vessel Technol. **133**, 051,204 (2011)
13. Mirzaei, D.: A new low-cost meshfree method for two and three dimensional problems in elasticity. Appl. Math. Model. **39**, 7181–7196 (2015)
14. Mirzaei, D., Hasanpour, K.: Direct meshless local Petrov–Galerkin method for elastodynamic analysis. Acta Mech. **227**, 619–632 (2016)
15. Mirzaei, D., Schaback, R.: Direct meshless local Petrov–Galerkin (DMLPG) method: a generalized MLS approximation. Appl. Numer. Math. **33**, 73–82 (2013)
16. Mirzaei, D., Schaback, R., Dehghan, M.: On generalized moving least squares and diffuse derivatives. IMA J. Numer. Anal. **32**, 983–1000 (2012)
17. Nickell, R.E., Sackman, J.J.: Approximate solutions in linear, coupled thermoelasticity. J. Appl. Mech. **35**, 255–266 (1968)
18. Nowacki, W.: Thermo-Elasticity, 2nd edn. Pergamon Press, New York (1986)

19. Prevost, J.H., Tao, D.: Finite element analysis of dynamic coupled thermoelasticity problems with relaxation times. J. Appl. Mech. Trans. ASME **50**, 817–822 (1983)
20. Qian, L.F., Batra, R.C.: Transient thermoelastic deformations of thick functionally graded plate. J. Therm. Stresses **27**, 705–740 (2004)
21. Shahani, A.R., Bashusqeh, S.M.: Analytical solution of the coupled thermo-elasticity problem in a pressurized sphere. J. Therm. Stresses **36**, 1283–1307 (2013)
22. Shahani, A.R., Bashusqeh, S.M.: Analytical solution of the thermoelasticity problem in a pressurized thickwalled sphere subjected to transient thermal loading. Math. Mech. Solids **19**, 135–151 (2014)
23. Sladek, J., Sladek, V., Atluri, S.N.: A pure contour formulation for meshless local boundary integral equation method in thermoelasticity. CMES-Comput. Model. Eng. Sci. **2**, 423–434 (2001)
24. Sladek, J., Sladek, V., Solek, P., Tan, C.L., Zhang, C.: Two- and three-dimensional transient thermoelastic analysis by the MLPG method. CMES-Comput. Model. Eng. Sci. **47**, 61–95 (2009)
25. Sladek, V., Sladek, J.: Boundary integral equation method in thermoelasticity, part I: general analysis. Appl. Math. Model. **7**, 241–253 (1984)
26. Suh, I.G., Tosaka, N.: Application of the boundary elment method to three dimensioanl linear coupled thermoelasticity problems. Theor. Appl. Mech. **38**, 169–175 (1989)
27. Tamma, K.K., Railkar, S.B.: On heat displacement based hybrid transfinite element formulations for uncoupled/coupled thermally induced stress wave propagation. J. Comput. Struct. **30**, 1025–1036 (1988)
28. Tanaka, M., Tanaka, K.: A boundary element approach to dynamic problems in coupled thermoelasticity. SM Arch. **6**, 467–491 (1981)
29. Ting, E.C., Chen, H.C.: A unified numerical approach for thermal stress waves. Comput. Struct. **15**, 165–175 (1982)
30. Tosaka, N., Suh, I.G.: Boundary elment analysis of dynamic coupled thermoelasticity problems. Comput. Mech. **8**, 331–342 (1991)
31. Wagner, P.: Fundamental matrix of the system of dynamic linear thermoelasticity. J. Therm. Stresses **17**, 549–565 (1994)
32. Wendland, H.: Scattered Data Approximation. Cambridge University Press, Cambridge (2005)
33. Zheng, B.J., Gao, X.W., Kai, Y., Zhang, C.Z.: A novel meshless local Petrov–Galerkin method for dynamic coupled thermoelasticity analysis under thermal and mechanical shock loading. Eng. Anal. Bound. Elem. **60**, 145–161 (2015)